

# An Evaluation of Simulated Precipitation Characteristics during OLYMPEX

ROBERT CONRICK AND CLIFFORD F. MASS

*Department of Atmospheric Sciences, University of Washington, Seattle, Washington*

(Manuscript received 10 July 2018, in final form 25 March 2019)

## ABSTRACT

The OLYMPEX field campaign, which took place around the Olympic Mountains of Washington State during winter 2015/16, provided data for evaluating the simulated microphysics and precipitation over and near that barrier. Using OLYMPEX observations, this paper assesses precipitation and associated microphysics in the WRF-ARW model over the U.S. Pacific Northwest. Model precipitation from the University of Washington real-time WRF forecast system during the OLYMPEX field program (November 2015–February 2016) and an extended period (2008–18) showed persistent underprediction of precipitation, reaching  $100 \text{ mm yr}^{-1}$  over the windward side of the coastal terrain. Increasing horizontal resolution does not substantially reduce this underprediction. Evaluating surface disdrometer observations during the 2015/16 OLYMPEX winter, it was found that the operational University of Washington WRF modeling system using Thompson microphysics poorly simulated the rain drop size distribution over a windward coastal valley. Although liquid water content was represented realistically, drop diameters were overpredicted, and, consequently, the rain drop distribution intercept parameter was underpredicted. During two heavy precipitation periods, WRF realistically simulated environmental conditions, including wind speed, thermodynamic structures, integrated moisture transport, and melting levels. Several microphysical parameterization schemes were tested in addition to the Thompson scheme, with each exhibiting similar biases for these two events. We show that the parameterization of aerosols over the coastal Northwest offered only minor improvement.

## 1. Introduction

The fidelity of model moist physics is a key issue for the operational numerical weather prediction community (Fritsch et al. 1998; Droegemeier et al. 2000). In much of the world, orographic precipitation provides substantial water resources, and therefore accurate simulations of precipitation and moist physics in terrain are crucial. A number of past field campaigns have examined moist physics in orography [e.g., the Cascade Project (Hobbs et al. 1971), CYCLES (Hobbs and Locatelli 1978), the Sierra Cooperative Pilot Project (Reynolds and Dennis 1986), CASPII (Cober et al. 1995), WISP (Rasmussen et al. 1992), MAP (Binder et al. 1996), and IMPROVE (Stoelinga et al. 2003)], but limitations in observing capabilities reduced their ability to evaluate parameterizations in mesoscale models. To address these limitations and to serve as ground validation for the NASA Precipitation Measurement Mission satellite for the Global Precipitation Mission (Hou et al. 2014; Skofronick-Jackson et al. 2017), the OLYMPEX field program was conducted during the

winter of 2015/16. A variety of midlatitude frontal systems were sampled during OLYMPEX by an extensive collection of satellite, aircraft, surface, and radar observations that provided a comprehensive microphysical description of these systems. Additional details of the OLYMPEX field campaign are found in Houze et al. (2017).

Ice microphysics impact the fidelity of simulated orographic precipitation (e.g., Hobbs et al. 1973; Rutledge and Hobbs 1983; Reisner et al. 1998; Gilmore et al. 2004), and the understanding of ice microphysics has improved based on observations from several field campaigns. As a result, model representation of snow has become more accurate, particularly with respect to snow shape and assumed size distributions (e.g., Colle and Zeng 2004; Colle et al. 2005; Woods et al. 2007; Thompson et al. 2008; Milbrandt et al. 2008; Lin and Colle 2009; Milbrandt et al. 2010). Riming parameterizations have also improved (e.g., Schoenberg Ferrier 1994; Myers et al. 1997; Geresdi 1998; Thompson et al. 2008; Milbrandt and Yau 2005; Morrison et al. 2009; Morrison and Grabowski 2010; Lin et al. 2013), with the most recent developments focusing on variable riming or single-category ice microphysics schemes (Morrison and Milbrandt 2015). Yet, deficiencies

---

*Corresponding author:* Robert Conrick, rconrick@uw.edu

DOI: 10.1175/JHM-D-18-0144.1

© 2019 American Meteorological Society. For information regarding reuse of this content and general copyright information, consult the [AMS Copyright Policy](#) ([www.ametsoc.org/PUBSReuseLicenses](http://www.ametsoc.org/PUBSReuseLicenses)).

do remain in the models, especially with regard to excessive snow production aloft (Conrick and Mass 2019).

Recent efforts have focused on improving the representation of cloud condensation nuclei (CCN) and ice nuclei (IN) in bulk microphysics schemes. Simulations of aerosol impacts on precipitation have found that a reduction in CCN can invigorate warm rain processes (Alizadeh-Choobari and Gharaylou 2017; Li et al. 2011; Khain 2009; Khain et al. 2012; Tao et al. 2012; Thompson and Eidhammer 2014; Nugent et al. 2016), which may be important along the relatively warm coastal areas of the Pacific Northwest, an area of generally low CCN concentrations. The impact of aerosols on midlatitude orographic precipitation may depend on location, precipitation intensity, and precipitation type. For instance, when exploring the impact of CCN on midlatitude orographic precipitation using a spectral bin model, Fan et al. (2014) showed that the introduction of dust aerosol to a pristine environment increased precipitation 10%–20% over the Sierra Nevada of California due to an enhancement of snow. For mixed-phase orographic precipitation, Fan et al. (2017) demonstrated that increasing aerosol concentrations downstream of the Sierra Nevada suppressed precipitation.

There have been several evaluations of the fidelity of simulated winter precipitation over the Pacific Northwest. Early studies by Colle et al. (1999) and Colle and Mass (2000) found overprediction of precipitation over the steep windward slopes of the Washington and Oregon Cascades, with underprediction in the lee of these barriers. In later work, Colle et al. (2000) demonstrated that light-to-moderate precipitation was overpredicted over windward slopes of Washington State, while heavy precipitation events were underpredicted. Similarly, during the IMPROVE experiment, overprediction was noted along windward slopes of the Oregon Cascades (Colle and Zeng 2004; Garvert et al. 2005a,b; Lin and Colle 2009). In contrast, Minder et al. (2008) found underprediction of extreme winter precipitation events over windward slopes of the coastal Olympic Mountains.

A limitation of past model evaluations was the lack of observations of rain drop size distributions (DSDs), which prevented precipitation biases from being explained in the context of simulated or observed DSDs. Furthermore, the extent to which aerosol concentrations may impact Pacific Northwest precipitation biases has not been explored, despite the potential susceptibility of precipitation in the Pacific Northwest to changes in aerosol concentrations (Joos et al. 2017). These issues are explored in this paper.

The aim of this study is to evaluate precipitation biases and low-level microphysics in the Weather Research and Forecasting (WRF) Model, comparing observed and simulated rain drop size distributions and precipitation

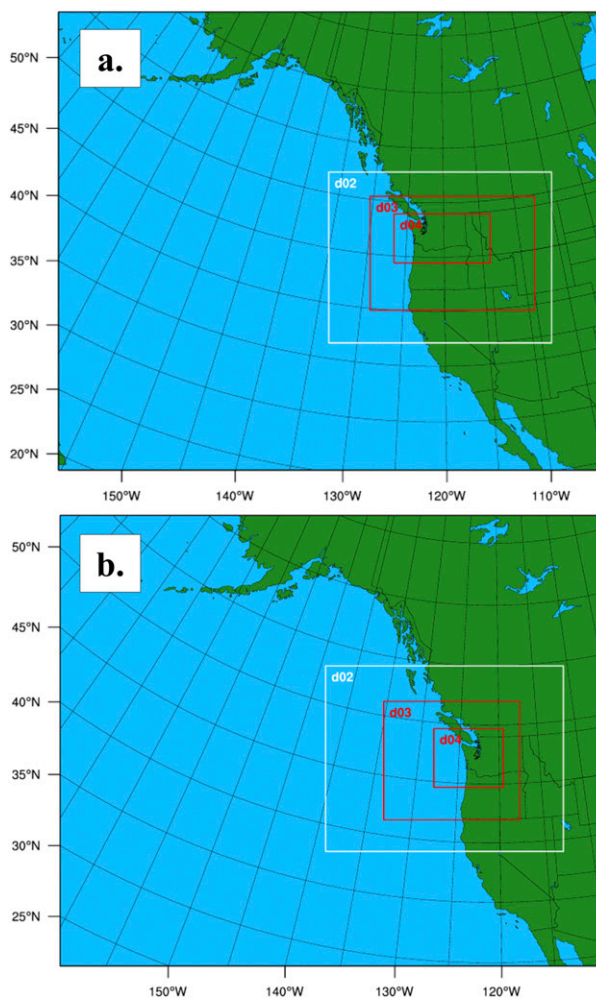


FIG. 1. The WRF-ARW domains used in this study: (a) the domain configuration of the UW real-time WRF during OLYMPEX, and (b) the domain configurations used in our microphysics and aerosol experiments. Labels d02, d03, and d04 indicate domains with 12-, 4-, and 1.33-km grid spacing, respectively.

during the OLYMPEX winter experiment and two heavy precipitation events. Our goal is to explore the following questions:

- 1) What biases exist in simulated precipitation over the Pacific Northwest in current microphysical parameterization schemes?
- 2) How do simulated rain characteristics (drop size distributions and number concentrations) vary as a function of precipitation forecast accuracy?
- 3) How does choice of microphysics scheme and CCN concentration affect simulated rain DSDs during two heavy precipitation events?

This paper is organized as follows: section 2 presents an overview of the model configuration. Results of a

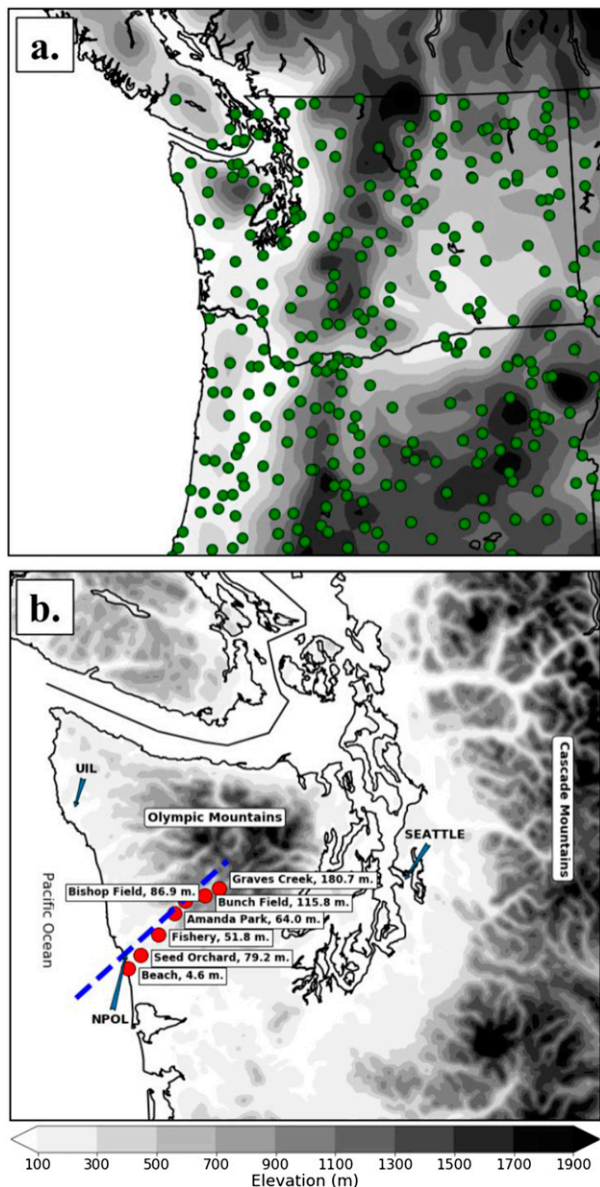


FIG. 2. Maps of observing stations used in (a) the extended-period analysis over the Pacific Northwest and (b) the OLYMPEX surface stations used to evaluate WRF during the 13 and 17 Nov events.

microphysical evaluation of real-time forecasts during the OLYMPEX winter are given in section 3, and two heavy precipitation events are documented in section 4. Finally, section 5 offers concluding remarks.

## 2. Model configurations and precipitation data

### a. Model configuration

During OLYMPEX, real-time operational forecasts were produced by the University of Washington (UW)

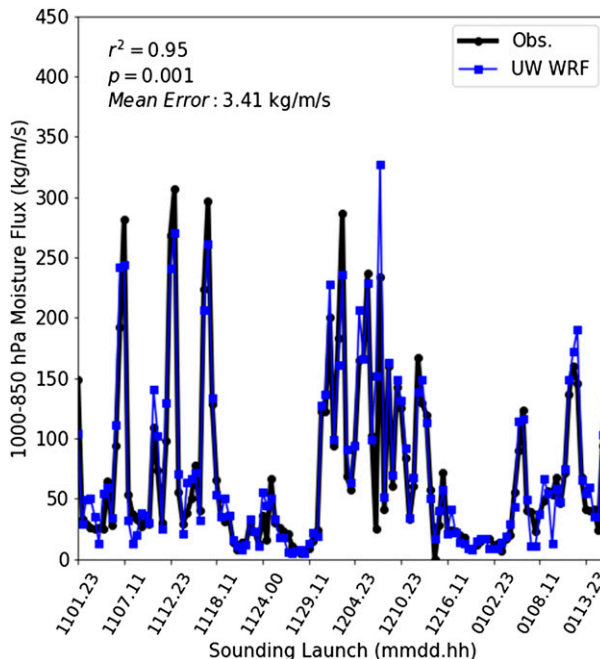


FIG. 3. The 1000–850-hPa moisture flux (IVT) observed at the UIL location compared to UW real-time WRF forecasts initialized daily at 0000 UTC for the November 2015–February 2016 OLYMPEX period.

using version 3.7.1 of the Advanced Research version of the WRF Model (WRF-ARW; Skamarock et al. 2008). A 36–12–4–1.33-km domain configuration was utilized with 38 vertical levels (Fig. 1a), with the innermost domain covering Washington State. Initialization and boundary conditions were driven by the 0.5° NOAA/National Weather Service (NWS) Global Forecast System (GFS) gridded forecasts, with some surface parameters initialized from other sources.<sup>1</sup> Boundaries were updated and the 36-km grid nudged every 3 h using the GFS forecasts. Parameterization options included the Noah-MP land surface model (Niu et al. 2011), the RRTMG radiation scheme (Iacono et al. 2008), the Yonsei University (YSU; Hong et al. 2006) boundary/surface layer (PBL) scheme, and Thompson microphysics (Thompson et al. 2008). A cumulus parameterization scheme (Grell–Freitas; Grell and Freitas 2014) is utilized for all but the 1.33-km domain.

For simulations of two heavy precipitation events that occurred during OLYMPEX, WRF-ARW version 3.8.1 was applied. The model configuration was identical to the operational configuration described previously, except for the following: 1) all simulations used a 36–12–4–1.33-km

<sup>1</sup> See the University of Washington online weather prediction portal for more information: <https://atmos.washington.edu/wrftrf/>.

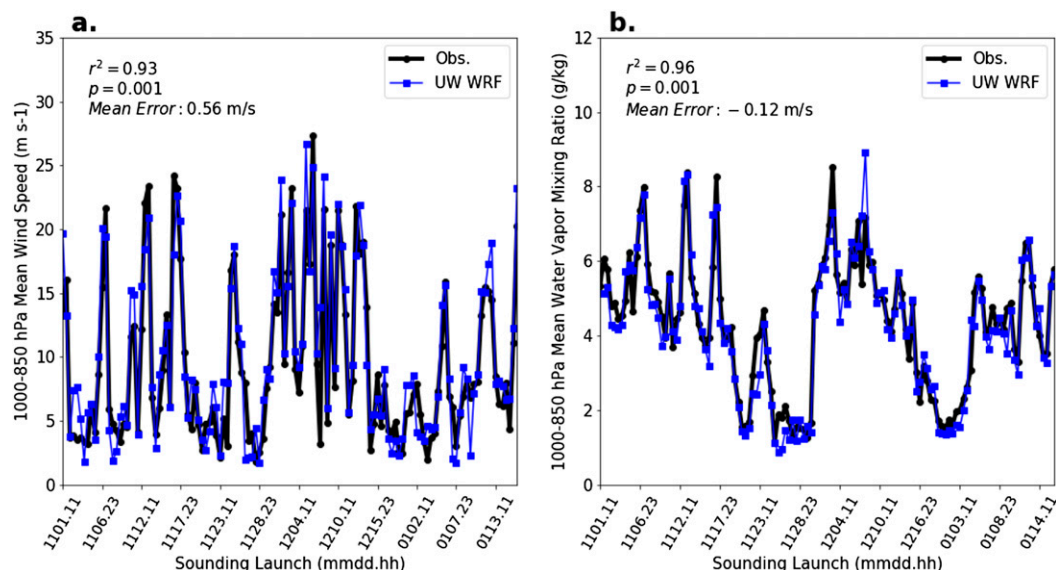


FIG. 4. The 1000–850-hPa mean (a) water vapor mixing ratios and (b) wind speed at the UIL location compared to UW real-time WRF forecasts initialized daily at 0000 UTC for the November 2015–February 2016 period.

domain configuration using 51 vertical levels, with the 1.33-km domain centered over the Olympic Peninsula (cf. Figs. 1a and 1b), and 2) 0.25° GFS gridded forecasts were used for initial and 3-h boundary conditions. Since new GFS runs are available every 6 h, only forecast hours 0 and 3 were used for boundary conditions and 36-km grid nudging. Simulations were conducted using a variety of microphysics schemes, including the Milbrandt–Yau double-moment (MY2; Milbrandt and Yau 2005), Morrison double-moment (MORR2; Morrison et al. 2009), P3 (Morrison and Milbrandt 2015), Stony Brook University (SBUYLIN; Lin and Colle 2011), Thompson (THOMP; Thompson et al. 2008), WSM6 (Hong and Lim 2006), and WDM6 (Lim and Hong 2010) schemes. Output from the 1.33-km domain was stored every 10 min.

#### b. Surface observations of rainfall

Precipitation data were obtained from the NWS Automated Surface Observing System (ASOS), the MesoWest cooperative mesonet (including RAWS sites; Horel et al. 2002), and OLYMPEX rain gauges. Figure 2a shows stations that were used for the analysis presented in section 3. WRF precipitation was interpolated to observation locations through a Cressman approach for the 36-, 12-, and 4-km domains and extracted from the nearest grid point for the 1.33-km domain.

Several OLYMPEX surface stations were utilized in our analyses (Fig. 2b). All sites had collocated dual tipping-bucket rain gauges and Parsivel disdrometers for capturing rain DSDs. These sites were calibrated and maintained during the OLYMPEX intensive observing

period to ensure optimal performance (Houze et al. 2017) and were within or near the Quinault Valley on the windward side of the Olympic Mountains. Following OLYMPEX, data were extensively reviewed by project personnel. Data that failed the quality control checks described below were removed. For microphysical evaluations, we analyzed the median volume diameter<sup>2</sup>  $D_0$ , liquid water content (LWC; the rainwater mass mixing ratio), and the normalized rain intercept parameter<sup>3</sup>  $N_w$  from the Parsivel units. These variables were chosen because they can be directly compared to model output and are necessary to describe rain drop size distributions.

Precipitation data from ASOS and RAWS rain gauge networks were quality controlled by removing excessively large values [6-h accumulation exceeding 15 in. (381 mm) or when 6-h accumulation was more than 3 in. (76 mm) greater than any other station within 100 km]. Days with more than 5% of hourly rainfall data missing were excluded from analysis. ASOS instruments undergo routine quality control and calibration procedures, including an extensive three-step routine involving built-in automated checks and inspection of observations by

<sup>2</sup> The median volume diameter  $D_0$  is defined as the diameter of a raindrop in a volume of air such that half the drops in that volume have a greater diameter and half have a smaller diameter.

<sup>3</sup> The  $N_w$  provides the ability to compare observed (gamma) drop size distributions with those from model microphysics schemes (gamma or exponential) and is directly related to the rain drop number concentration.

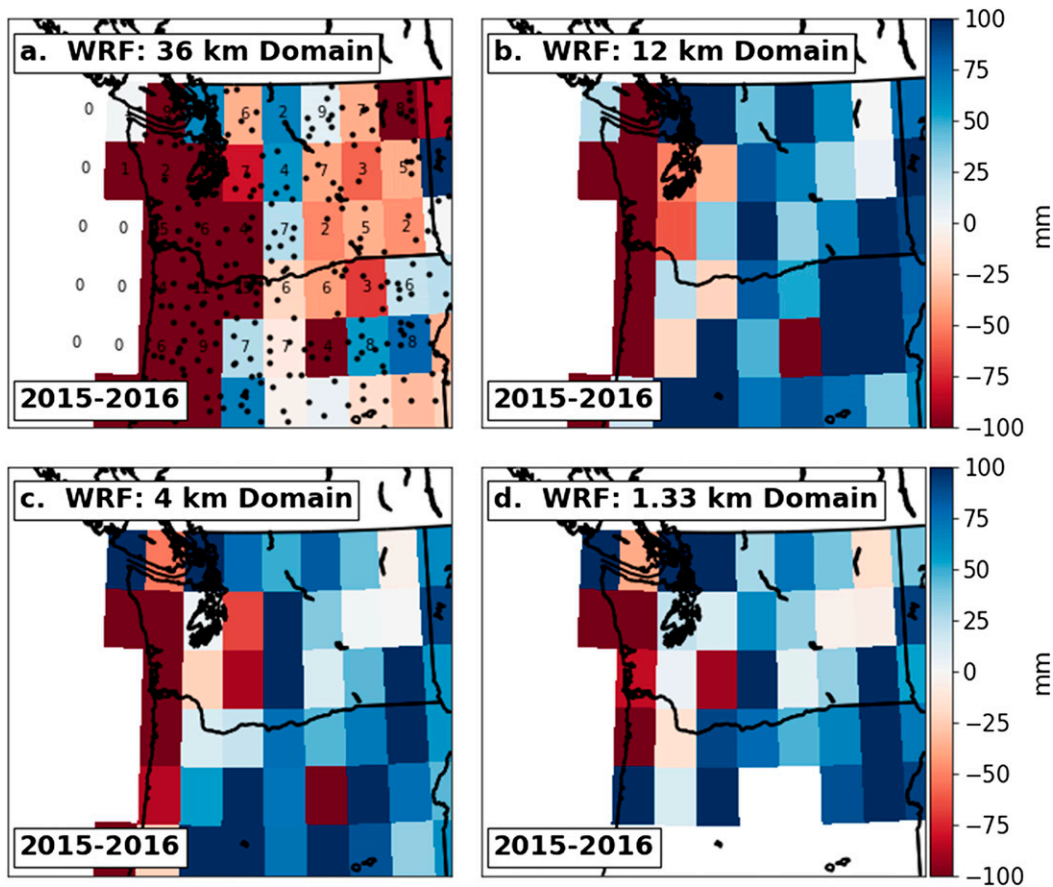


FIG. 5. Maps of forecast departure from observations of cumulative precipitation on a 1° grid during the November 2015–February 2016 period. Each panel shows this metric at (a)–(d) different UW WRF spatial resolutions. The numbers and location of each station are also indicated in (a).

NWS personnel.<sup>4</sup> Site visits are conducted if data appear suspect. The rain gauges deployed by NASA during OLYMPEX were tipping-bucket gauges from Met One, Inc. According to Petersen et al. (2017a), these gauges have an accuracy of  $\pm 0.5\%$  at  $13 \text{ mm h}^{-1}$  and  $\pm 1\%$  at  $25\text{--}75 \text{ mm h}^{-1}$ . The Parsivel disdrometers, also deployed by NASA, were quality controlled in the field as part of the data acquisition process (Petersen et al. 2017b), beginning with removal of data associated with rain rates less than  $0.01 \text{ mm h}^{-1}$  or less than 10 drops. To eliminate potentially erroneous drop counts, a threshold is employed to remove drops if their fall velocity is not within 50% of the terminal fall velocity of an identically sized drop as computed from Beard (1976). Finally, in processing the data, we exclude Parsivel data if more than 5% of data are missing during a 10-min averaging period.

Determining the sampling uncertainty of OLYMPEX instruments is an important step toward model comparison. Because we are using operational data, it is difficult to reliably quantify sampling uncertainty without multiple collocated measurements. However, there have been a number of studies, many by NASA personnel, which have assessed the uncertainty of these instruments. Wang et al. (2008) found that measurements from NASA tipping-bucket gauges are more accurate ( $<15\%$  mean relative absolute error) when data are considered over periods greater than 7 min, which is shorter than the period we analyze. Tokay et al. (2010) compared the accuracy of collocated ASOS, RAWS, and NASA gauges using a year of precipitation data. Their key findings were that NASA gauge biases were less than 10%, while ASOS and RAWS gauges had errors less than 15%. The sampling uncertainty of  $D_0$  and number concentration from collocated Parsivel disdrometers was documented by Jaffrain and Berne (2011), who demonstrated that number concentration uncertainty was less than 5%

<sup>4</sup> The ASOS user manual outlines the procedures taken to ensure quality ASOS data. For more information see <https://www.weather.gov/media/asos/aum-toc.pdf>.

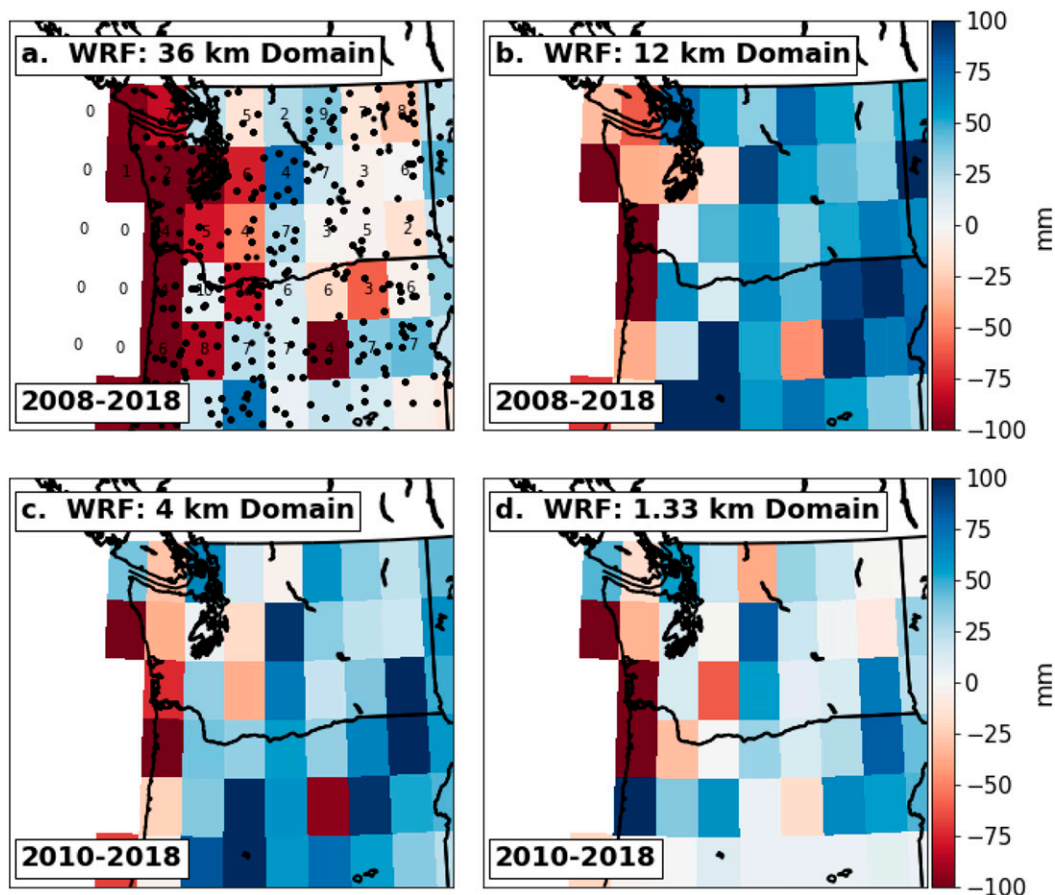


FIG. 6. As in Fig. 5, but considering average annual wintertime (November–February) forecast departures over the 2008–18 period. Note the differing periods considered for the 4- and 1.33-km domains.

and  $D_0$  uncertainty less than 7% at temporal averages exceeding 10 min. Thus, there is confidence that the observing systems used in this study are sufficiently accurate for model evaluation.

### 3. Results of OLYMPEX wintertime simulations

#### a. Fidelity of incoming moisture flux during the OLYMPEX project

Before evaluating model microphysics, it is important to evaluate the fidelity of the coastal winds and incoming moisture, since they play a controlling role on moist physics. For example, vertically integrated moisture flux [integrated water vapor transport (IVT)] is strongly correlated with U.S. West Coast orographic precipitation (Neiman et al. 2008; Lin et al. 2013) and is a key parameter in defining and forecasting atmospheric rivers (e.g., Newell et al. 1992; Zhu and Newell 1998). Furthermore, IVT forecast errors have been shown to correlate with precipitation errors (Lin et al. 2013).

To determine whether the simulated flow and IVT impinging on the Olympic Peninsula during OLYMPEX are accurate, the 1000–850-hPa IVT from the UW real-time WRF forecasts initialized at 0000 UTC for forecast hours 6–24 were compared against observed values from rawinsondes at Quillayute (UIL) during the November 2015–February 2016 period (Fig. 3). There is excellent agreement ( $r^2 = 0.95$ ;  $p < 0.001$ ) over the entire period, with a mean error of  $3.41 \text{ kg m}^{-1} \text{ s}^{-1}$ . Figure 4 shows 1000–850-hPa mean wind speed and water vapor mixing ratio, the constituents of IVT, during the same period. As with IVT, results show excellent agreement between observations and simulations ( $r^2 = 0.9$ ;  $p < 0.001$ ). Thus, the low-level simulated synoptic environment appears to agree well with observations during the OLYMPEX period.

#### b. Extended precipitation evaluation

Figure 5 presents gridded cumulative precipitation forecast errors across the Pacific Northwest based on the UW WRF forecasts from November 2015 to February

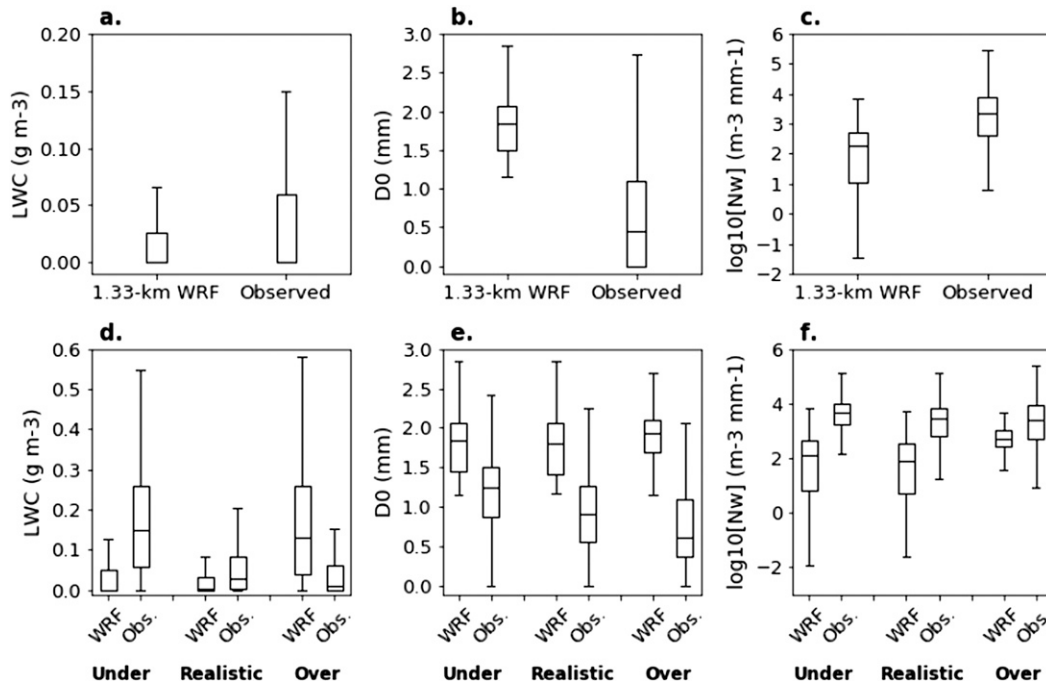


FIG. 7. Boxplots showing the distributions of (a) LWC, (b)  $D_0$ , and (c)  $N_w$  data during the period November 2015–November 2016. (d)–(f) As in (a)–(c), but subdivided by when precipitation rate is realistically simulated ( $\pm 0.5 \text{ mm h}^{-1}$  error), underpredicted (error  $< -0.5 \text{ mm h}^{-1}$ ), or overpredicted (error  $> 0.5 \text{ mm h}^{-1}$ ).

2016. Forecasts were initialized daily at 0000 UTC, and forecast hours 6–24 were analyzed by interpolating model output to individual stations within each  $1^\circ$  box and computing a mean cumulative precipitation forecast error for that box.

Along the Pacific coastal zone and over the windward slopes of the coastal terrain there was considerable underprediction for the 36-km grid, with cumulative errors exceeding 100 mm. This underprediction was modestly reduced as grid spacing was decreased from 36 to 12 km, with little improvement at 4- and 1.33-km grid spacing. For the remainder of the region, overprediction generally dominated, particularly inland along the windward slopes of the Oregon Cascades and east of the Cascade crest. To further evaluate winter precipitation bias, a decade (2008–18) of winter precipitation forecasts from WRF was analyzed (Fig. 6), showing a similar result: coastal underprediction and inland overprediction regardless of model resolution.

A relevant question is whether these results are influenced by gauge undercatch. Over higher terrain and east of the Cascades crest, it is reasonable to expect most winter precipitation reaching the ground would be snow instead of rain, and thus gauge undercatch may be of concern, particularly during strong winds (Rasmussen et al. 2012). However, over the Pacific coastal zone, where freezing levels typically vary between 800 and

2800 m during winter storms (Lundquist et al. 2008), nearly all precipitation reaching the surface is rain, and is thus less impacted by undercatch. This is particularly true during anomalously warm atmospheric river events with an average melting level of approximately 2300 m (Zagrodnik et al. 2018).

*c. Microphysical evaluation during the OLYMPEX winter*

Surface-based microphysical observations during OLYMPEX were mainly located on the windward (western) slopes of the Olympic Mountains in the Quinalt River Valley. In an effort to understand why winter underprediction is prevalent over the coastal zone, we consider liquid-phase microphysics data from Parsivel disdrometers and rainfall from collocated tipping-bucket rain gauges (sites shown in Fig. 2b). To compute mean drop diameter  $D_0$  and the normalized rain intercept parameter  $N_w$ , we used the formulations from Thompson et al. (2008), and to produce an accurate comparison to observations, we limited the calculations to the size range of the Parsivel ( $D \geq 0.25 \text{ mm}$ ). The analysis considered the UW WRF forecasts initialized daily at 0000 UTC from November 2015 to February 2016 and forecast hours 6–24 were used.

Figure 7 shows boxplots of LWC,  $D_0$ , and  $N_w$  from the OLYMPEX surface stations. When considering all data

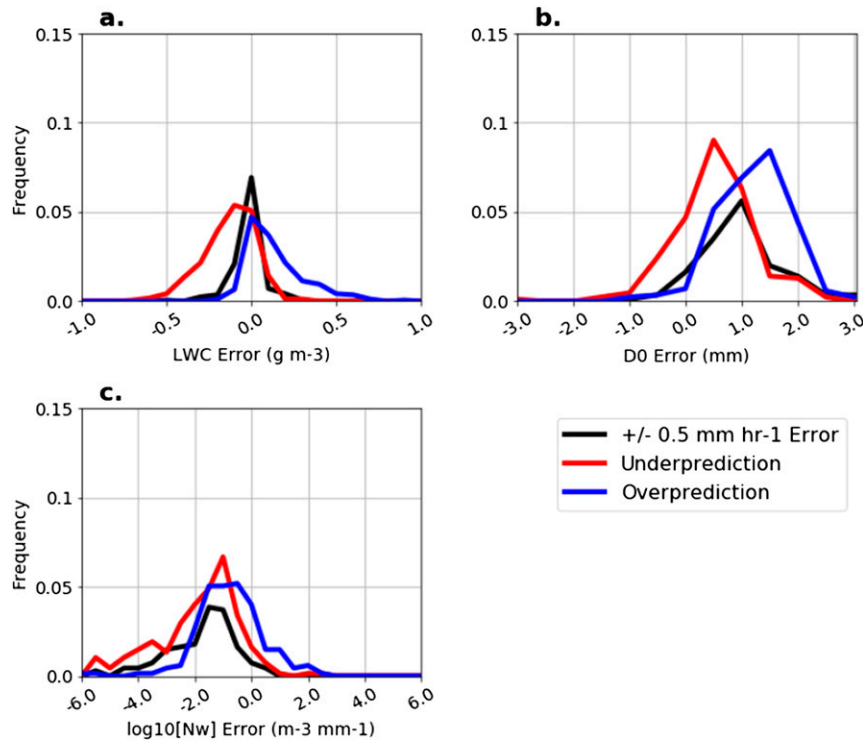


FIG. 8. As in Fig. 7, but showing frequency distributions of simulated errors of (a) LWC, (b)  $D_0$ , and (c)  $N_w$  over the period November 2015–November 2016 when precipitation rate is realistically simulated ( $\pm 0.5 \text{ mm h}^{-1}$  error), underpredicted (error  $< -0.5 \text{ mm h}^{-1}$ ), or overpredicted (error  $> 0.5 \text{ mm h}^{-1}$ ).

(Figs. 7a–c), simulated LWC was within the bounds of observations, though smaller and with a narrower range of values than observed. Model  $D_0$  is substantially larger than observed, while simulated  $N_w$  is modestly less than observations. We further divided the data into three categories: realistic precipitation prediction (rain rate error within  $0.5 \text{ mm h}^{-1}$  of observed), overprediction of rain rate (positive error exceeding  $0.5 \text{ mm h}^{-1}$ ), and underprediction of rain rate (negative error exceeding  $0.5 \text{ mm h}^{-1}$ ). Not surprisingly, LWC is underpredicted when model precipitation is low, and vice versa. The  $D_0$  is larger and  $N_w$  smaller in WRF than in the observations, regardless of how well rain rate is predicted. Simulated  $D_0$  agrees better with observations when rain rate is underpredicted,  $N_w$  is best simulated when rain rate is overpredicted.

Figure 8 shows frequency distributions of forecast errors of LWC,  $D_0$ , and  $N_w$  from the OLYMPEX surface stations. Consistent with Fig. 7d, the underprediction of LWC corresponds to underpredicted rain rates, while excessive prediction of LWC corresponded to overpredicted rates. Turning to model  $D_0$  and  $N_w$  (Figs. 8b,c), it appears that realistic rain rates resulted from compensating errors: mean  $D_0$  was 1.16 mm larger than observed, while the mean  $N_w$  was 62% smaller than

observed. Underpredicted rain rates generally resulted from  $D_0$  being modestly larger than observed and  $N_w$  lower than observed. Overprediction of precipitation was associated with much larger than observed  $D_0$  and less negatively skewed  $N_w$ . From these error distributions, we demonstrate that rain characteristics vary considerably when rain rate is over, under, or realistically forecast.

Table 1 examines whether the distributions in Fig. 8 of errors of LWC,  $D_0$ , and  $N_w$  during periods of under and overpredicted rain rates are statistically different from periods when rain rate is realistic. At a 95% confidence threshold, all tests indicate statistical significance except 1)  $D_0$  when rain rate is realistically predicted compared to  $D_0$  when rain rate is overpredicted, and 2)  $N_w$  during periods of realistic rain rates compared to  $N_w$  during underpredicted rain rates.

#### 4. Heavy precipitation periods

During OLYMPEX, several midlatitude cyclones and associated fronts impacted the Olympic Mountains, with the warm sector of some of these events including strong, warm, moist air flows (i.e., atmospheric rivers; Newell et al. 1992; Zhu and Newell 1994, 1998;

TABLE 1. Statistical significance scores ( $p$  values) of the results of Welch's  $t$  test, in which one distribution is inspected to determine whether it is significantly different than another distribution. The table considers distributions of  $D_0$ ,  $N_w$ , and LWC when precipitation rate is realistically ( $\pm 5 \text{ mm h}^{-1}$  error) simulated compared to when precipitation rate is overpredicted or underpredicted during the November 2015–February 2016 period. Statistically significant results (95% confidence) are italicized.

	Underprediction	Overprediction
LWC	<0.001	<0.001
$D_0$	<0.001	0.373
$N_w$	0.459	<0.001

Ralph et al. 2004). Atmospheric rivers result in considerable hydrologic impacts in the Pacific Northwest, including extreme precipitation and flooding (Neiman et al. 2011; Warner et al. 2012). In the next sections, simulations of two atmospheric river events are examined

to investigate 1) what biases in precipitation and liquid-phase microphysics are associated with atmospheric rivers, 2) how other microphysical parameterization schemes perform during these events, and 3) whether the parameterization of aerosols impacts precipitation and microphysics during these events.

a. Cases studies: 13 and 17 November 2015

The first event (13 November) included a modest atmospheric river that reached the Olympic Peninsula. The 850-hPa synoptic chart at 1200 UTC 13 November (Fig. 9a) indicates a low over the Gulf of Alaska, with strong (45 kt;  $1 \text{ kt} \approx 0.51 \text{ m s}^{-1}$ ) 850-hPa flow impacting the west coast of North America. The warm sector of this system was characterized by high IVT and a moist-neutral environment, with substantial vertical shear in the lower troposphere (Fig. 9b). Following cold frontal passage, precipitation intensity declined in the

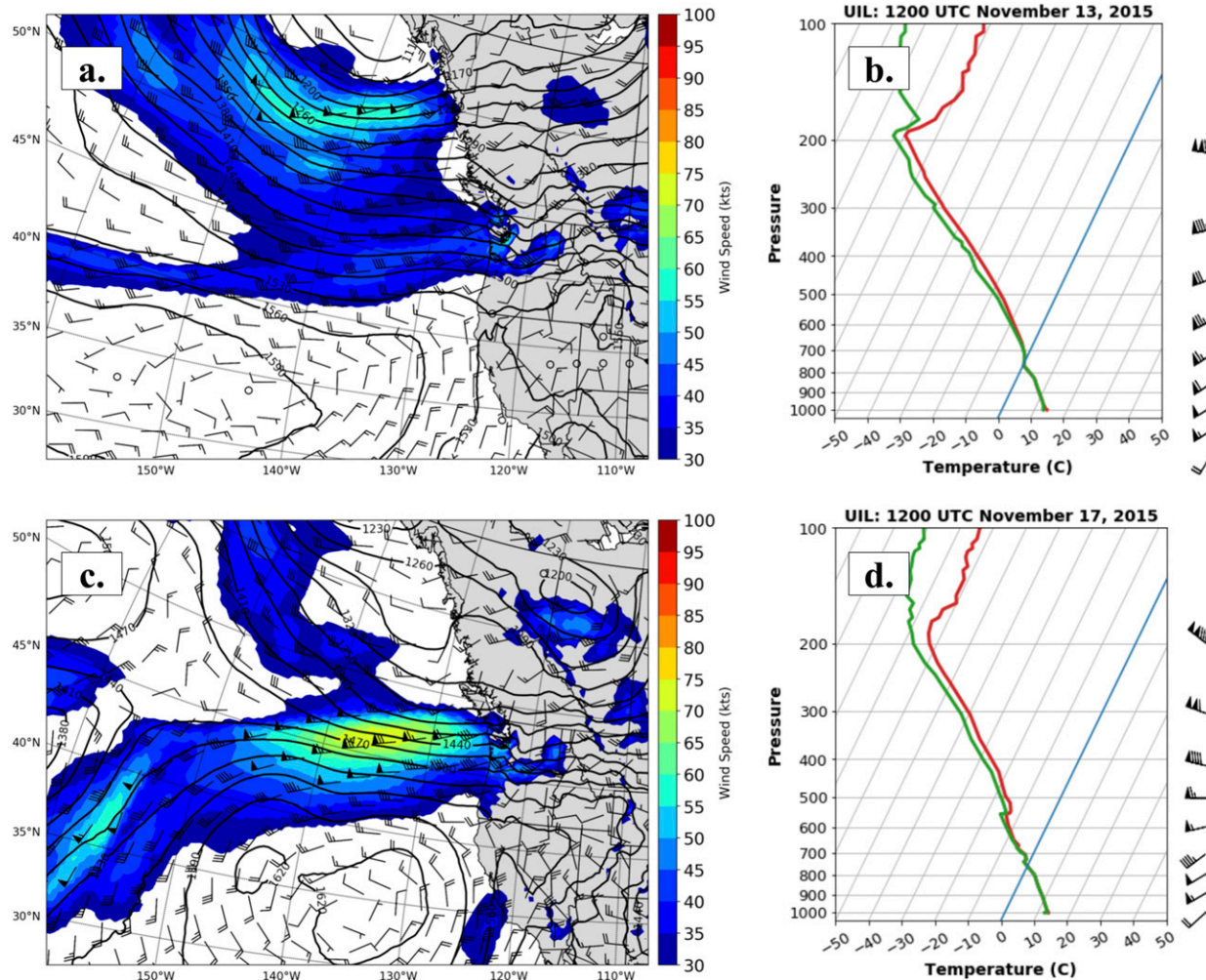


FIG. 9. (a) The 850-hPa NARR analyzed geopotential height and wind and (b) UIL sounding, both valid at 1200 UTC 13 Nov 2015. (c),(d) As in (a) and (b), but valid at 1200 UTC 17 Nov 2015.

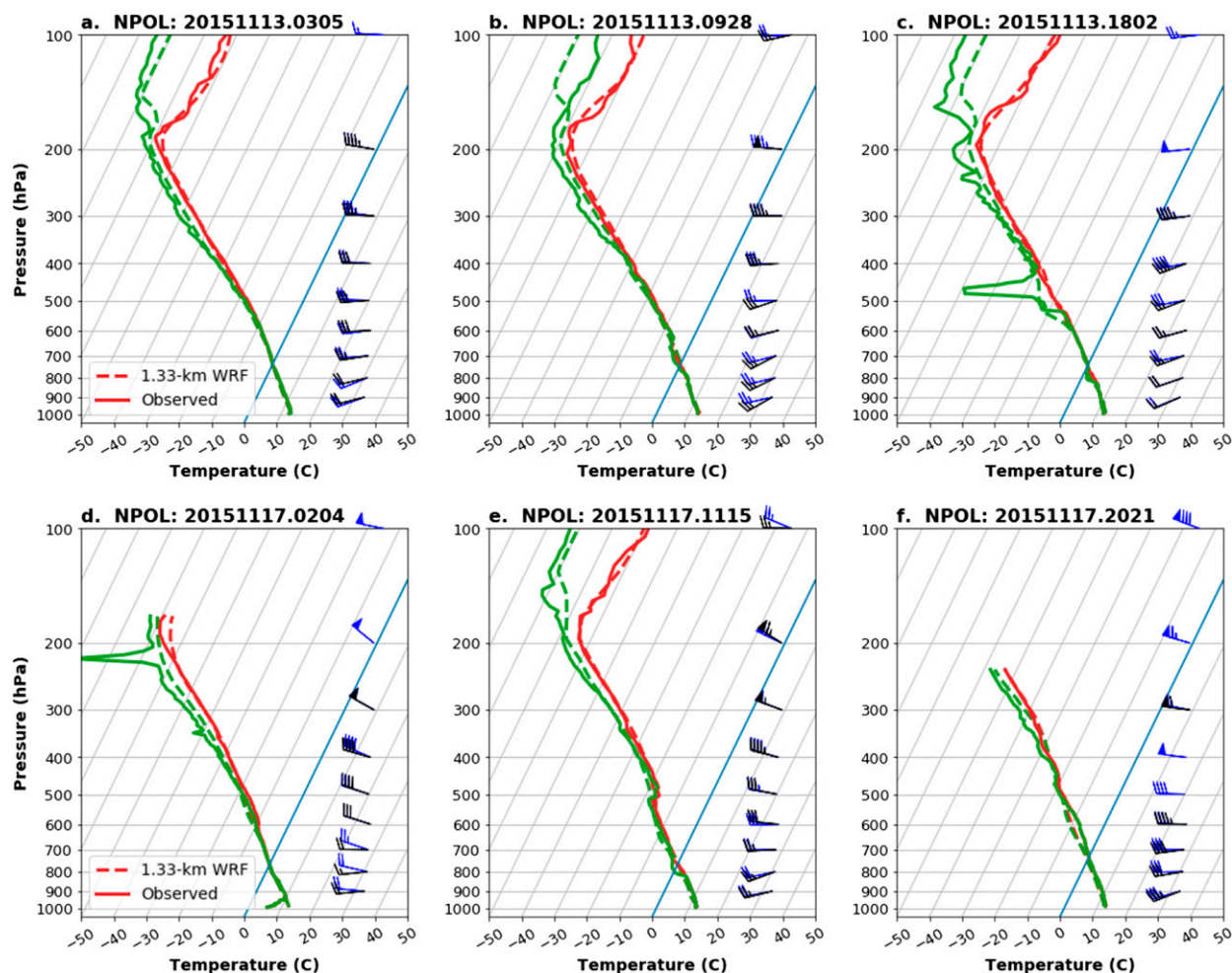


FIG. 10. Observed and simulated rawinsonde profiles at the NPOL site for selected times during the (a)–(c) 13 Nov 2015 and (d)–(f) 17 Nov 2015 cases. The red line represents the temperature profile, and the green line denotes the dewpoint temperature profile. Solid profiles indicate observed values; dashed lines show the 1.33-km WRF simulation. Black wind barbs are observed values; blue wind barbs are from the WRF model.

postfrontal convection. Accumulations in the windward Quinault River valley exceeded 300 mm during the 24-h period ending 0000 UTC 14 November, which includes the warm period of the event. Following Zagrodnik et al. (2018), we define the atmospheric river period as 0300–1800 UTC 13 November.

The second event occurred on 17 November 2015 and was associated with a shortwave trough embedded in strong westerly flow (Fig. 9c). At 1200 UTC 17 November, strong (45 kt) southwesterly 850-hPa flow approached the Olympic Mountains. Prior to cold frontal passage around 2200 UTC, over 200 mm of precipitation was observed on the windward slopes of the Olympics (Fig. 9d). For this event, we define the atmospheric river period as 0000–2000 UTC 17 November, derived from radar observations and soundings launched at the NASA dual-polarization S-band radar (NPOL) site.

In the Quinault Valley, approximately 5%–10% of the total winter precipitation during OLYMPEX occurred during these two events.

Both atmospheric river periods were characterized by moist–neutral conditions throughout the troposphere, which WRF simulated accurately. Figure 10 shows observed and simulated rawinsonde profiles for 13 November (Figs. 10a–c) and 17 November (Figs. 10d–f). For both cases, only minor differences exist between observed and simulated environmental temperature and moisture profiles, wind speed and direction, and the height of the 0°C level. This confirms that the model realistically captured the environmental conditions during these periods.

Further, it is relevant to ask whether the model convective scheme, used on the 36-, 12-, and 4-km domains, may have contributed to precipitation or environmental

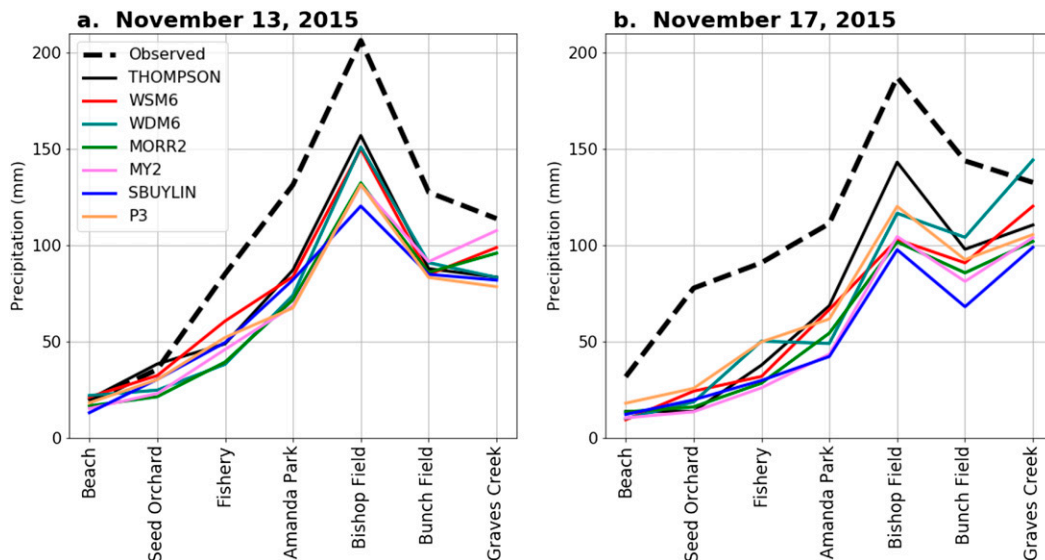


FIG. 11. Observed and simulated total precipitation accumulation at 1.33-km grid spacing from several microphysical schemes at the Quinault River Valley OLYMPLEX observing sites in Fig. 2b for warm “atmospheric river” periods of the (a) 13 Nov and (b) 17 Nov events. Distance from the Pacific Ocean increases to the right in each panel.

errors in the 1.33-km domain. For the 13 and 17 November events, the convective scheme produced only 1.68% and 0.78%, respectively, of the total precipitation in the 4-km domain. Most of this impact is offshore and well to the southwest of the Olympic Peninsula. Thus, it appears that the convective parameterization on the coarse domains was infrequently activated and likely had little impact on precipitation in the higher-resolution domains.

*b. Precipitation and microphysics evaluations*

Precipitation in the windward Quinault Valley was generally underpredicted during the heavy precipitation events of 13 and 17 November 2015. Figure 11 shows a transect along the line in Fig. 2b of precipitation accumulations from observations and simulations using a variety of WRF microphysics schemes during these heavy precipitation periods. Simulated precipitation totals at locations near the coast (Beach) and farthest inland (Graves Creek) agreed best with observations. At other locations, there was substantial underprediction, with simulations at Bishop Field underpredicting by nearly 100 mm for 13 November and 75 mm during 17 November. None of the microphysics schemes performed consistently better than others. For the 13 November event, all simulations produced a peak in precipitation accumulation at the correct location (Bishop Field), while in the 17 November case several schemes erroneously produced maximum precipitation at Graves Creek.

Figure 12 presents frequency distributions of LWC,  $D_0$ , and  $N_w$  during both events at the Quinault Valley

stations (Fig. 2b) for various microphysics parameterizations used. When precipitation rate was underpredicted,  $D_0$  was too large, while LWC and  $N_w$  were too small. Accurate LWC was noted when precipitation rates were realistic, despite large  $D_0$ . The P3 scheme, using a single ice category, underpredicted LWC while producing excessively large  $D_0$ . Other notable results include the following:

- 1) WDM6 and P3 produced a peak LWC error of  $-0.45\text{g kg}^{-1}$ , which was the largest error among the schemes.
- 2) WDM6 had very low  $N_w$  compared to observations, due in part to the low LWC.
- 3) Thompson produced the most accurate LWC and  $D_0$  forecasts, though its  $N_w$  differed little from the other schemes tested.

*c. Impact of aerosols*

Because the concentration of CCN in the generally clean air reaching the Olympic Peninsula during the winter has been observed to be approximately  $50\text{ cm}^{-3}$  (Hegg et al. 1991) and most bulk microphysics schemes (i.e., Thompson et al. 2008) typically parameterize maritime CCN using  $100\text{ cm}^{-3}$ , it is possible that poor representations of CCN concentrations and the associated processes contributed to the rain biases during the heavy precipitation events of 13 and 17 November 2015. In low CCN environments, cloud droplets will be larger and less numerous, which invigorates warm-rain processes by enhancing the rate of autoconversion from cloud droplets to rain, and therefore enhances drop

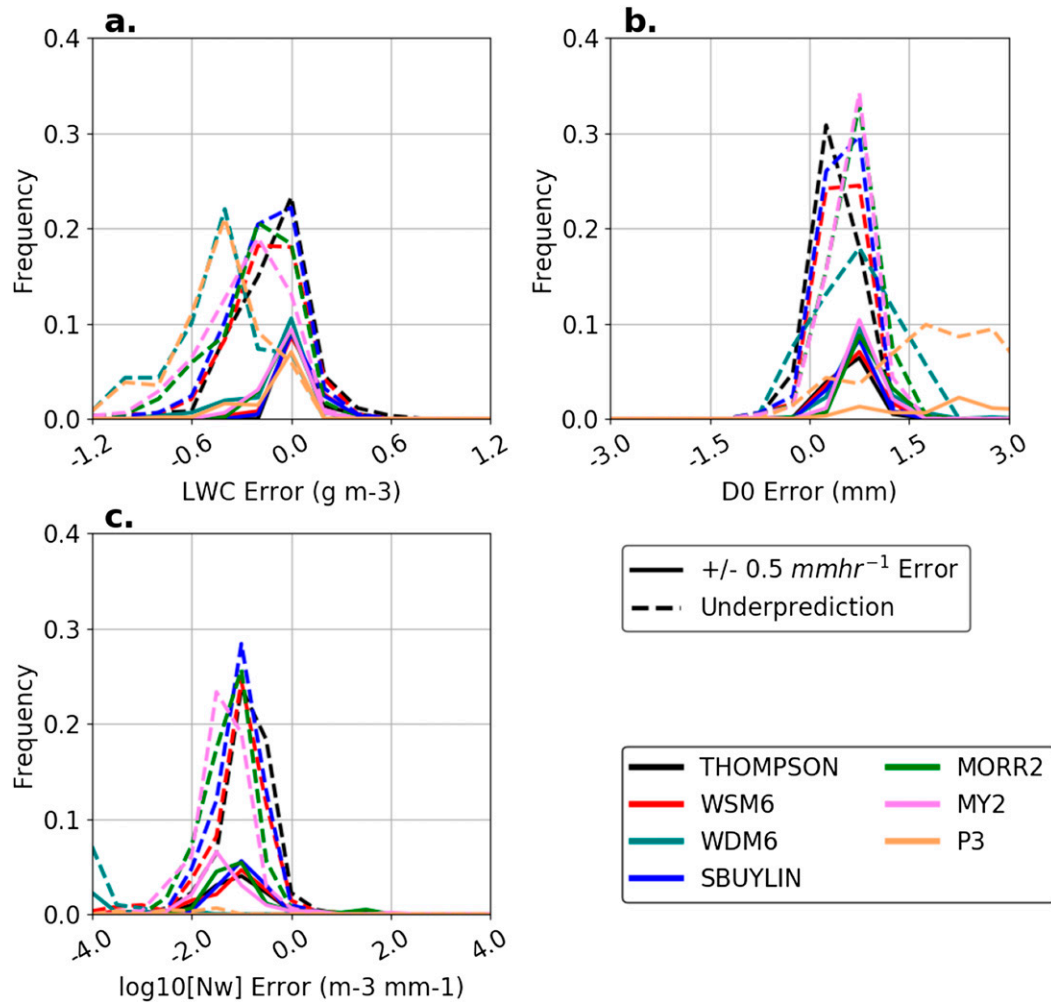


FIG. 12. Frequency distributions of simulated errors of (a) LWC, (b)  $D_0$ , and (c)  $N_w$ , combined over the 13 and 17 Nov heavy precipitation events when precipitation rate is accurately predicted ( $\pm 0.5 \text{ mm h}^{-1}$  error) and underpredicted (error  $< -0.5 \text{ mm h}^{-1}$ ).

collision-coalescence and breakup. Thompson and Eidhammer (2014) noted this impact on rain microphysics in a simulated midlatitude cyclone, which caused an increase in rainwater content. Applying their finding to the Quinault Valley, we hypothesize that a simulated environment with fewer CCN may reduce the aforementioned biases in rain DSDs during atmospheric river events.

In the default configuration of the Thompson microphysics scheme, the cloud droplet number concentration, which can be considered as the CCN concentration, is set to a constant value of  $100 \text{ cm}^{-3}$ . We perform an exceptionally “clean” simulation using  $25 \text{ cm}^{-3}$  for cloud droplet concentration, and compare it to our control simulation using the default  $100 \text{ cm}^{-3}$ . Compared to the control simulation, clean simulation precipitation accumulations in the Quinault Valley

were minimally changed during the two heavy precipitation events (Fig. 13). During the 13 November event, some increase in precipitation is noted at Bishop Field in the clean simulation, though less rain falls closer to the coast; the 17 November event exhibits the opposite characteristics. In both cases, precipitation accumulations are generally altered by less than 10%.

Figure 14 shows that the simulated vertical profiles of rain and cloud water mixing ratios during these two events were more sensitive than precipitation to the prescribed cloud droplet concentration, particularly in the lowest kilometer of the atmosphere. The difference between the clean and control experiments was smallest at the Beach site and increased at higher elevations in the Quinault Valley. At Bishop Field, the clean configuration produced  $0.6 \text{ g kg}^{-1}$  of rainwater mixing ratio at

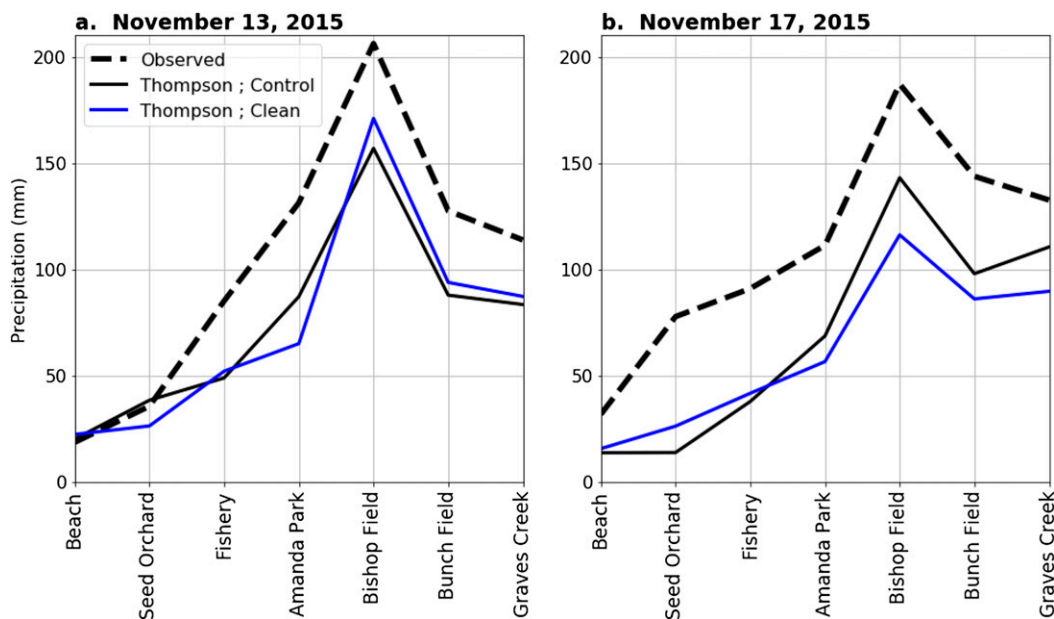


FIG. 13. As in Fig. 11, but displaying precipitation totals from the CCN concentration experiments.

the surface, compared to  $0.4 \text{ g kg}^{-1}$  in the control run. In addition, cloud water mixing ratios decreased in the clean simulation. We hypothesize that enhanced warm rain processes contributed to the clean simulation's increase of rainwater mixing ratio, as in Thompson and Eidhammer (2014).

Figure 15 shows mean profiles of  $D_0$ ,  $N_w$ , and LWC during the heavy precipitation periods. At all sites, a smaller number of prescribed cloud droplets were associated with an increase in LWC and a decrease in  $D_0$ , which increased  $N_w$ . This behavior ultimately offset the biases previously discussed and is consistent with simulations in Thompson and Eidhammer (2014). The implication for these findings is that a reduction in model aerosols in this region may reduce the DSD biases previously described, but may not improve accumulated precipitation totals.

## 5. Discussion and concluding remarks

The topography of the Pacific Northwest plays a crucial role in the region's water resources, with orographic precipitation accounting for a considerable fraction of winter precipitation. The OLYMPEX field campaign during the 2015/16 winter over the Olympic Mountains of Washington State provided a comprehensive set of observations for evaluating microphysics in mesoscale models. In this work, we utilized data from surface rain gauges and Parsivel disdrometers to describe errors in simulated rain drop size distribution characteristics and precipitation.

During the period of November 2015–February 2016, spatial errors of forecast precipitation from the University of Washington WRF mesoscale modeling system were examined. The results generally agreed with past studies in the Pacific Northwest, finding overprediction of precipitation on the windward slopes of the Oregon Cascades and considerable underprediction along the Pacific coastal zone. Errors in rain drop size distributions during this period showed significant overprediction of rain drop median volume diameter  $D_0$  and resultant underprediction of the normalized drop intercept parameter  $N_w$  regardless of whether precipitation rates were realistically forecast. We further analyzed simulated precipitation from 2008 to 2018, with results indicating underprediction along and near the Pacific coast, with little improvement when model resolution was increased.

To examine precipitation and rain microphysics biases during heavy precipitation periods, two atmospheric river events (13 and 17 November 2015) from the OLYMPEX winter were simulated using a variety of moist physics schemes and compared to observations from the Quinault River Valley, located on the windward side of the Olympics. Both events were shown to have environments that were well simulated by WRF, including thermodynamic structure and the height of the freezing level. Underprediction of precipitation was prevalent at sites in the valley from near sea level to high on the windward slopes. No particular scheme generally produced a more accurate precipitation forecast than the control (Thompson et al. (2008)

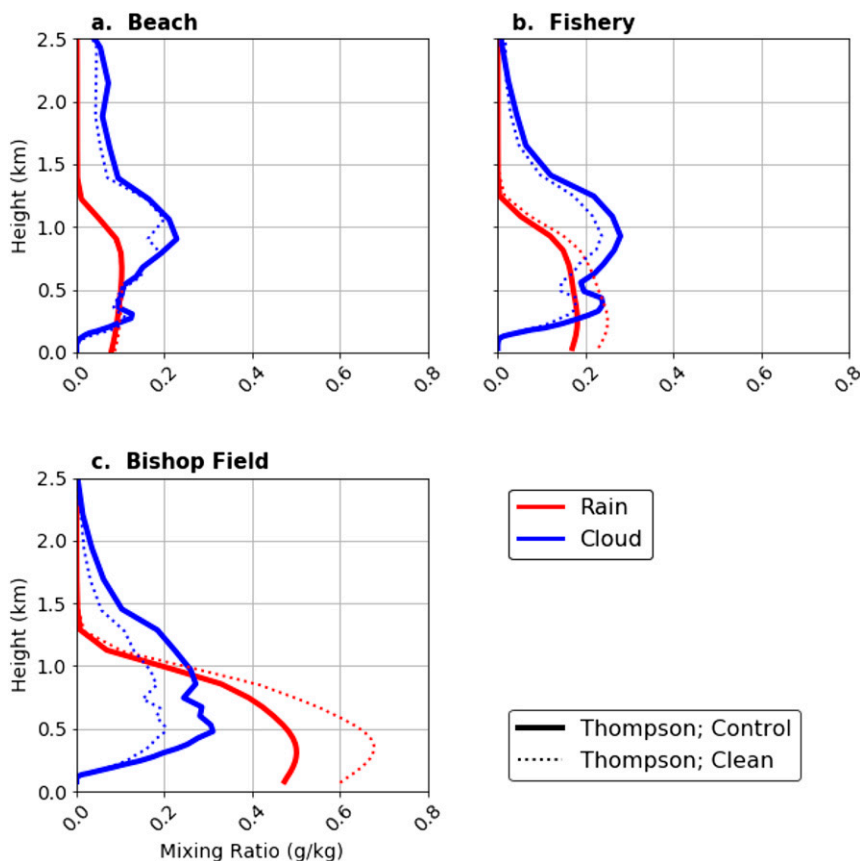


FIG. 14. Vertical profiles of rainwater and cloud water mixing ratios at Quinault Valley stations, averaged over both events for the clean and control experiments.

scheme). Furthermore, model rain microphysical parameters ( $D_0$ ,  $N_w$ , and LWC) exhibited overprediction of  $D_0$  and corresponding underprediction of  $N_w$ .

Because the airflow impinging upon the Olympic Mountains during the cool season has been observed to be clean in terms of CCN/aerosol concentrations (Hegg et al. 1991); furthermore, existing literature suggests that a reduction in simulated aerosol concentrations leads to an increase in LWC and decrease in  $D_0$  as a result of enhanced warm rain processes (Thompson and Eidhammer 2014). Thus, we examined the impact of a clean environment on precipitation and microphysics in the Quinault Valley during the two heavy precipitation events. This experiment used the Thompson microphysics scheme with an exceptionally clean aerosol value of  $25 \text{ cm}^{-3}$  for the prescribed cloud droplet number concentration, in contrast to  $100 \text{ cm}^{-3}$  for the control run. The reduction in cloud droplets favored more accurate rain DSDs that had larger LWC, smaller  $D_0$ , and correspondingly larger  $N_w$ . However, despite these changes, precipitation totals were nearly unchanged by the more realistic CCN concentrations.

The deep, saturated environment and the presence of a brightband signature in observations from NPOL during the events of 13 and 17 November 2015 confirm the occurrence of melting ice hydrometeors in simulations and observations. Thus, even with high melting levels which often exceeded 2000 m, there were still ice processes occurring aloft and potentially influencing precipitation accumulations. However, it is important to note that the presence of melting ice and a brightband signature does not preclude the occurrence or dominance of warm-rain processes near the surface, as was often the case during OLYMPEX (Zagrodnik et al. 2018). Indeed, the small median volume diameters seen in Parsivel observations during OLYMPEX indicate that warm-rain processes dominated the drop size spectra through condensation and collision-coalescence. Conversely, we hypothesize that WRF may be deficient in simulating warm-rain processes over this region.

The errors found in rain DSDs are problematic and exist in even the most sophisticated bulk microphysics schemes. Because drop size and intercept parameters influence the majority of rain microphysical processes in bulk schemes, it is reasonable to assume that such

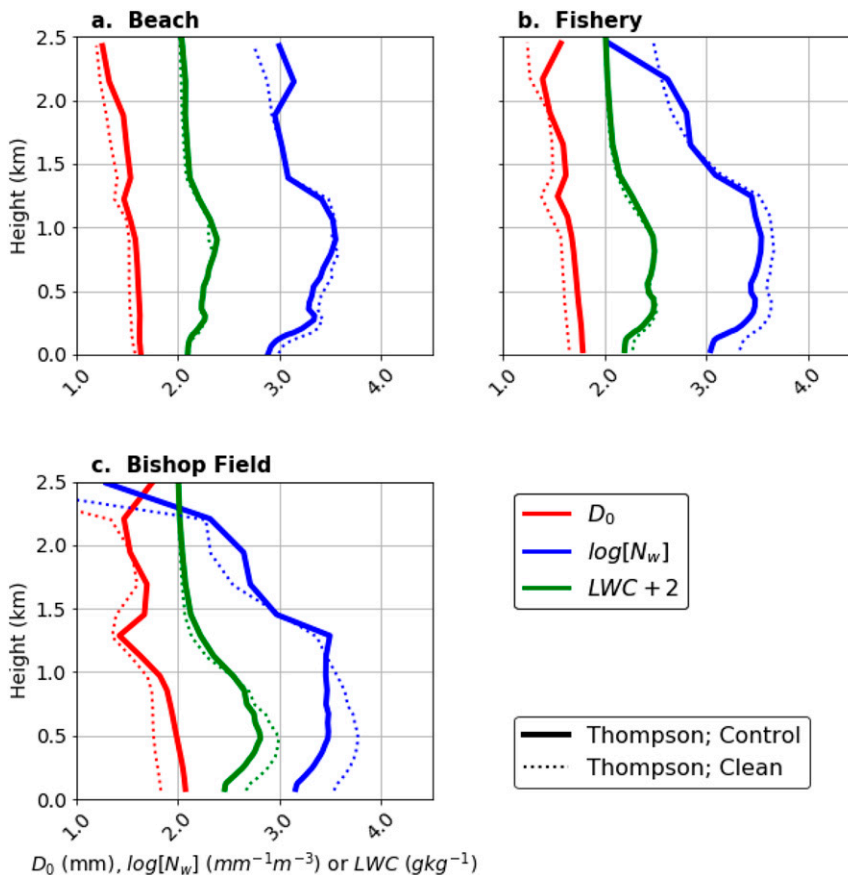


FIG. 15. Vertical profiles of  $D_0$ ,  $\log(N_w)$ , and LWC at Quinault Valley stations, averaged over both events for the clean and control experiments. LWC is offset on the graph in order to enhance readability.

errors may result in poor process rates in microphysical parameterizations. For example, diameter and LWC are the input values to most sedimentation (fallout) parameterizations, which impact the spatial distribution of precipitation. Our future work will examine such deficiencies in microphysical processes and their potential impact on precipitation forecast accuracy in this region.

*Acknowledgments.* This work is supported by the National Science Foundation through Grant AGS-1349847. The authors thank Dr. Greg Thompson for providing useful insights on this research, and two anonymous reviewers for their suggestions which helped to greatly improve the manuscript.

REFERENCES

Alizadeh-Choobari, O., and M. Gharaylou, 2017: Aerosol impacts on radiative and microphysical properties of clouds and precipitation formation. *Atmos. Res.*, **185**, 53–64, <https://doi.org/10.1016/j.atmosres.2016.10.021>.

Beard, K. V., 1976: Terminal velocity and shape of cloud and precipitation drops aloft. *J. Atmos. Sci.*, **33**, 851–864, [https://doi.org/10.1175/1520-0469\(1976\)033<0851:TVASOC>2.0.CO;2](https://doi.org/10.1175/1520-0469(1976)033<0851:TVASOC>2.0.CO;2).

Binder, P., and Coauthors, 1996: MAP—Mesoscale Alpine Programme design proposal. MAP Programme Office, 77 pp. [Available from MAP Programme Office c/o Swiss Meteorological Institute, Krähbühlstrasse 58, CH-8044 Zürich, Switzerland.]

Cober, S. G., G. A. Isaac, and J. W. Strapp, 1995: Aircraft icing measurements in east coast winter storms. *J. Appl. Meteor.*, **34**, 88–100, <https://doi.org/10.1175/1520-0450-34.1.88>.

Colle, B. A., and C. F. Mass, 2000: The 5–9 February 1996 flooding event over the Pacific Northwest: Sensitivity studies and evaluation of the MM5 precipitation forecasts. *Mon. Wea. Rev.*, **128**, 593–617, [https://doi.org/10.1175/1520-0493\(2000\)128<0593:TFFEOT>2.0.CO;2](https://doi.org/10.1175/1520-0493(2000)128<0593:TFFEOT>2.0.CO;2).

—, and Y. Zeng, 2004: Bulk microphysical sensitivities within the MM5 for orographic precipitation. Part I: The Sierra 1986 event. *Mon. Wea. Rev.*, **132**, 2780–2801, <https://doi.org/10.1175/MWR2821.1>.

—, K. J. Westrick, and C. F. Mass, 1999: Evaluation of MM5 and Eta-10 precipitation forecasts over the Pacific Northwest during the cool season. *Wea. Forecasting*, **14**, 137–154, [https://doi.org/10.1175/1520-0434\(1999\)014<0137:EOMAEP>2.0.CO;2](https://doi.org/10.1175/1520-0434(1999)014<0137:EOMAEP>2.0.CO;2).

- , C. F. Mass, and K. J. Westrick, 2000: MM5 precipitation verification over the Pacific Northwest during the 1997–99 cool seasons. *Wea. Forecasting*, **15**, 730–744, [https://doi.org/10.1175/1520-0434\(2000\)015<0730:MPVOTP>2.0.CO;2](https://doi.org/10.1175/1520-0434(2000)015<0730:MPVOTP>2.0.CO;2).
- , M. F. Garvert, J. B. Wolfe, C. F. Mass, and C. P. Woods, 2005: The 13–14 December 2001 IMPROVE-2 event. Part III: Simulated microphysical budgets and sensitivity studies. *J. Atmos. Sci.*, **62**, 3535–3558, <https://doi.org/10.1175/JAS3552.1>.
- Conrick, R., and C. F. Mass, 2019: Evaluating simulated microphysics during OLYMPEX Using GPM satellite observations. *J. Atmos. Sci.*, **76**, 1093–1105, <https://doi.org/10.1175/JAS-D-18-0271.1>.
- Droegemeier, K. K., and Coauthors, 2000: Hydrological aspects of weather prediction and flood warnings: Report of the Ninth Prospectus Development Team of the U.S. Weather Research Program. *Bull. Amer. Meteor. Soc.*, **81**, 2665–2680, [https://doi.org/10.1175/1520-0477\(2000\)081<2653:EFITST>2.3.CO;2](https://doi.org/10.1175/1520-0477(2000)081<2653:EFITST>2.3.CO;2).
- Fan, J., and Coauthors, 2014: Aerosol impacts on California winter clouds and precipitation during CalWater 2011: Local pollution versus long-range transported dust. *Atmos. Chem. Phys.*, **14**, 81–101, <https://doi.org/10.5194/acp-14-81-2014>.
- , L. R. Leung, D. Rosenfeld, and P. J. DeMott, 2017: Effects of cloud condensation nuclei and ice nucleating particles on precipitation processes and supercooled liquid in mixed-phase orographic clouds. *Atmos. Chem. Phys.*, **17**, 1017–1035, <https://doi.org/10.5194/acp-17-1017-2017>.
- Fritsch, J. M., and Coauthors, 1998: Quantitative precipitation forecasting: Report of the Eighth Prospectus Development Team, U.S. Weather Research Program. *Bull. Amer. Meteor. Soc.*, **79**, 285–299, [https://doi.org/10.1175/1520-0477\(1998\)079<0285:QPFROT>2.0.CO;2](https://doi.org/10.1175/1520-0477(1998)079<0285:QPFROT>2.0.CO;2).
- Garvert, M. F., B. A. Colle, and C. F. Mass, 2005a: The 13–14 December 2001 IMPROVE-2 event. Part I: Synoptic and mesoscale evolution and comparison with a mesoscale model simulation. *J. Atmos. Sci.*, **62**, 3474–3492, <https://doi.org/10.1175/JAS3549.1>.
- , C. P. Woods, B. A. Colle, C. F. Mass, P. V. Hobbs, M. T. Stoelinga, and J. B. Wolfe, 2005b: The 13–14 December 2001 IMPROVE-2 event. Part II: Comparisons of MM5 model simulations of clouds and precipitation with observations. *J. Atmos. Sci.*, **62**, 3520–3534, <https://doi.org/10.1175/JAS3551.1>.
- Geresdi, I., 1998: Idealized simulation of the Colorado hailstorm case: Comparison of bulk and detailed microphysics. *Atmos. Res.*, **45**, 237–252, [https://doi.org/10.1016/S0169-8095\(97\)00079-3](https://doi.org/10.1016/S0169-8095(97)00079-3).
- Gilmore, M. S., J. M. Straka, and E. N. Rasmussen, 2004: Precipitation and evolution sensitivity in simulated deep convective storms: Comparisons between liquid-only and simple ice and liquid phase microphysics. *Mon. Wea. Rev.*, **132**, 1897–1916, [https://doi.org/10.1175/1520-0493\(2004\)132<1897:PAESIS>2.0.CO;2](https://doi.org/10.1175/1520-0493(2004)132<1897:PAESIS>2.0.CO;2).
- Grell, G. A., and S. R. Freitas, 2014: A scale and aerosol aware stochastic convective parameterization for weather and air quality modeling. *Atmos. Chem. Phys.*, **14**, 5233–5250, <https://doi.org/10.5194/acp-14-5233-2014>.
- Hegg, D. A., L. F. Radke, and P. V. Hobbs, 1991: Measurements of Aitken nuclei and cloud condensation nuclei in the marine atmosphere and their relation to the DMS-cloud-climate hypothesis. *J. Geophys. Res.*, **96**, 18 727–18 733, <https://doi.org/10.1029/91JD01870>.
- Hobbs, P. V., and J. D. Locatelli, 1978: Rainbands, precipitation cores and generating cells in a cyclonic storm. *J. Atmos. Sci.*, **35**, 230–241, [https://doi.org/10.1175/1520-0469\(1978\)035<0230:RPCAGC>2.0.CO;2](https://doi.org/10.1175/1520-0469(1978)035<0230:RPCAGC>2.0.CO;2).
- , and Coauthors, 1971: Studies of winter cyclonic storms over the Cascade Mountains (1970–71). Research Rep. VI, Cloud Physics Group, Atmospheric Sciences Department, University of Washington, 306 pp.
- , R. C. Easter, and A. B. Fraser, 1973: A theoretical study of the flow of air and fallout of solid precipitation over mountainous terrain: Part II. Microphysics. *J. Atmos. Sci.*, **30**, 813–823, [https://doi.org/10.1175/1520-0469\(1973\)030<0813:ATSOTF>2.0.CO;2](https://doi.org/10.1175/1520-0469(1973)030<0813:ATSOTF>2.0.CO;2).
- Hong, S.-Y., and J.-O. J. Lim, 2006: The WRF single-moment 6-class microphysics scheme (WSM6). *J. Korean Meteor. Soc.*, **42**, 129–151.
- , Y. Noh, and J. Dudhia, 2006: A new vertical diffusion package with an explicit treatment of entrainment processes. *Mon. Wea. Rev.*, **134**, 2318–2341, <https://doi.org/10.1175/MWR3199.1>.
- Horel, J., and Coauthors, 2002: Mesowest: Cooperative mesonets in the western United States. *Bull. Amer. Meteor. Soc.*, **83**, 211–225, [https://doi.org/10.1175/1520-0477\(2002\)083<0211:MCMITW>2.3.CO;2](https://doi.org/10.1175/1520-0477(2002)083<0211:MCMITW>2.3.CO;2).
- Hou, A. Y., and Coauthors, 2014: The Global Precipitation Measurement Mission. *Bull. Amer. Meteor. Soc.*, **95**, 701–722, <https://doi.org/10.1175/BAMS-D-13-00164.1>.
- Houze, R. A., Jr., and Coauthors, 2017: The Olympic Mountains Experiment (OLYMPEX). *Bull. Amer. Meteor. Soc.*, **98**, 2167–2188, <https://doi.org/10.1175/BAMS-D-16-0182.1>.
- Iacono, M. J., J. S. Delamere, E. J. Mlawer, M. W. Shephard, S. A. Clough, and W. D. Collins, 2008: Radiative forcing by long-lived greenhouse gases: Calculations with the AER radiative transfer models. *J. Geophys. Res.*, **113**, D13103, <https://doi.org/10.1029/2008JD009944>.
- Jaffrain, J., and A. Berne, 2011: Experimental quantification of the sampling uncertainty associated with measurements from PARSIVEL disdrometers. *J. Hydrometeorol.*, **12**, 352–370, <https://doi.org/10.1175/2010JHM1244.1>.
- Joos, H., E. Madonna, K. Witlox, S. Ferrachat, H. Wernli, and U. Lohmann, 2017: Effect of anthropogenic aerosol emissions on precipitation in warm conveyor belts in the western North Pacific in winter – A model study with ECHAM6-HAM. *Atmos. Chem. Phys.*, **17**, 6243–6255, <https://doi.org/10.5194/acp-17-6243-2017>.
- Khain, A. P., 2009: Notes on state-of-the art investigations of aerosol effects on precipitation: A critical review. *Environ. Res. Lett.*, **4**, 015004, <https://doi.org/10.1088/1748-9326/4/1/015004>.
- , V. Phillips, N. Benmoshe, and A. Pokrovsky, 2012: The role of small soluble aerosols in the microphysics of deep maritime clouds. *J. Atmos. Sci.*, **69**, 2787–2807, <https://doi.org/10.1175/2011JAS3649.1>.
- Li, Z., F. Niu, J. Fan, Y. Liu, D. Rosenfeld, and Y. Ding, 2011: Long-term impacts of aerosols on the vertical development of clouds and precipitation. *Nat. Geosci.*, **4**, 888–894, <https://doi.org/10.1038/ngeo1313>.
- Lim, K.-S. S., and S.-Y. Hong, 2010: Development of an effective double-moment cloud microphysics scheme with prognostic cloud condensation nuclei (CCN) for weather and climate models. *Mon. Wea. Rev.*, **138**, 1587–1612, <https://doi.org/10.1175/2009MWR2968.1>.
- Lin, Y., and B. A. Colle, 2009: The 4–5 December 2001 IMPROVE-2 event: Observed microphysics and comparisons with the Weather Research and Forecasting Model. *Mon. Wea. Rev.*, **137**, 1372–1392, <https://doi.org/10.1175/2008MWR2653.1>.
- , and —, 2011: A new bulk microphysical scheme that includes riming intensity and temperature-dependent ice

- characteristics. *Mon. Wea. Rev.*, **139**, 1013–1035, <https://doi.org/10.1175/2010MWR3293.1>.
- , —, and S. E. Yuter, 2013: Impact of moisture flux and freezing level on simulated orographic precipitation errors over the Pacific Northwest. *J. Hydrometeorol.*, **14**, 140–152, <https://doi.org/10.1175/JHM-D-12-019.1>.
- Lundquist, J. D., P. J. Neiman, B. E. Martner, A. B. White, D. J. Gattas, and F. M. Ralph, 2008: Rain versus snow in the Sierra Nevada, California: Comparing Doppler profiling radar and surface observations of melting level. *J. Hydrometeorol.*, **9**, 194–211, <https://doi.org/10.1175/2007JHM853.1>.
- Meyers, M. P., R. L. Walko, J. Y. Harrington, and W. R. Cotton, 1997: New RAMS cloud microphysics. Part II: The two-moment scheme. *Atmos. Res.*, **45**, 3–39, [https://doi.org/10.1016/S0169-8095\(97\)00018-5](https://doi.org/10.1016/S0169-8095(97)00018-5).
- Milbrandt, J. A., and M. K. Yau, 2005: A multimoment bulk microphysics parameterization. Part I: Analysis of the role of the spectral shape parameter. *J. Atmos. Sci.*, **62**, 3051–3064, <https://doi.org/10.1175/JAS3534.1>.
- , —, J. Mailhot, and S. Bélair, 2008: Simulation of an orographic precipitation event during IMPROVE-2. Part I: Evaluation of the control run using a triple-moment bulk microphysics scheme. *Mon. Wea. Rev.*, **136**, 3873–3893, <https://doi.org/10.1175/2008MWR2197.1>.
- , —, —, —, and R. McTaggart-Cowan, 2010: Simulation of an orographic precipitation event during IMPROVE-2. Part II: Sensitivity to the number of moments in the bulk microphysics scheme. *Mon. Wea. Rev.*, **138**, 625–642, <https://doi.org/10.1175/2009MWR3121.1>.
- Minder, J. R., D. R. Durran, G. H. Roe, and A. M. Anders, 2008: The climatology of small-scale orographic precipitation over the Olympic Mountains: Patterns and processes. *Quart. J. Roy. Meteor. Soc.*, **134**, 817–839, <https://doi.org/10.1002/qj.258>.
- Morrison, H., and W. W. Grabowski, 2010: An improved representation of rimed snow and conversion to graupel in a multicomponent bin microphysics scheme. *J. Atmos. Sci.*, **67**, 1337–1360, <https://doi.org/10.1175/2010JAS3250.1>.
- , and J. A. Milbrandt, 2015: Parameterization of cloud microphysics based on the prediction of bulk ice particle properties. Part I: Scheme description and idealized tests. *J. Atmos. Sci.*, **72**, 287–311, <https://doi.org/10.1175/JAS-D-14-0065.1>.
- , G. Thompson, and V. Tatarskii, 2009: Impact of cloud microphysics on the development of trailing stratiform precipitation in a simulated squall line: Comparison of one- and two-moment schemes. *Mon. Wea. Rev.*, **137**, 991–1007, <https://doi.org/10.1175/2008MWR2556.1>.
- Neiman, P. J., F. M. Ralph, G. A. Wick, J. D. Lundquist, and M. D. Dettlinger, 2008: Meteorological characteristics and overland precipitation impacts of atmospheric rivers affecting the west coast of North America based on eight years of SSM/I satellite observations. *J. Hydrometeorol.*, **9**, 22–47, <https://doi.org/10.1175/2007JHM855.1>.
- , L. J. Schick, F. M. Ralph, M. Hughes, and G. A. Wick, 2011: Flooding in western Washington: The connection to atmospheric rivers. *J. Hydrometeorol.*, **12**, 1337–1358, <https://doi.org/10.1175/2011JHM1358.1>.
- Newell, R. E., N. E. Newell, Y. Zhu, and C. Scott, 1992: Tropospheric rivers?—A pilot study. *Geophys. Res. Lett.*, **19**, 2401–2404, <https://doi.org/10.1029/92GL02916>.
- Niu, G.-Y., and Coauthors, 2011: The community Noah land surface model with multiparameterization options (Noah-MP): 1. Model description and evaluation with local-scale measurements. *J. Geophys. Res.*, **116**, D12109, <https://doi.org/10.1029/2010JD015139>.
- Nugent, A. D., C. D. Watson, G. Thompson, and R. B. Smith, 2016: Aerosol impacts on thermally driven orographic convection. *J. Atmos. Sci.*, **73**, 3115–3132, <https://doi.org/10.1175/JAS-D-15-0320.1>.
- Petersen, W. A., D. B. Wolff, J. Wang, and A. Tokay, 2017a: GPM Ground Validation Met One Rain Gauge Pairs OLYMPEX. NASA Global Hydrology Resource Center Distributed Active Archive Center, accessed 15 April 2018, <https://doi.org/10.5067/GPMGV/OLYMPEX/GAUGES/DATA201>.
- Petersen, W. A., A. Tokay, P. N. Gatlin, and M. T. Wingo, 2017b: GPM Ground Validation Autonomous Parsivel Unit (APU) OLYMPEX. NASA Global Hydrology Resource Center Distributed Active Archive Center, accessed 15 April 2018, <https://doi.org/10.5067/GPMGV/OLYMPEX/APU/DATA301>.
- Ralph, F. M., P. J. Neiman, and G. A. Wick, 2004: Satellite and CALJET aircraft observations of atmospheric rivers over the eastern North Pacific Ocean during the winter of 1997/98. *Mon. Wea. Rev.*, **132**, 1721–1745, [https://doi.org/10.1175/1520-0493\(2004\)132<1721:SACAO>2.0.CO;2](https://doi.org/10.1175/1520-0493(2004)132<1721:SACAO>2.0.CO;2).
- Rasmussen, R., and Coauthors, 1992: Winter Icing and Storms Project (WISP). *Bull. Amer. Meteor. Soc.*, **73**, 951–974, [https://doi.org/10.1175/1520-0477\(1992\)073<0951:WIASP>2.0.CO;2](https://doi.org/10.1175/1520-0477(1992)073<0951:WIASP>2.0.CO;2).
- , and Coauthors, 2012: How well are we measuring snow: The NOAA/FAA/NCAR Winter Precipitation Test Bed. *Bull. Amer. Meteor. Soc.*, **93**, 811–829, <https://doi.org/10.1175/BAMS-D-11-00052.1>.
- Reisner, J., R. M. Rasmussen, and R. T. Bruintjes, 1998: Explicit forecasting of supercooled liquid water in winter storms using the MM5 mesoscale model. *Quart. J. Roy. Meteor. Soc.*, **124**, 1071–1107, <https://doi.org/10.1002/qj.49712454804>.
- Reynolds, D. W., and A. S. Dennis, 1986: A review of the Sierra Cooperative Pilot Project. *Bull. Amer. Meteor. Soc.*, **67**, 513–523, [https://doi.org/10.1175/1520-0477\(1986\)067<0513:AROTSC>2.0.CO;2](https://doi.org/10.1175/1520-0477(1986)067<0513:AROTSC>2.0.CO;2).
- Rutledge, S. A., and P. V. Hobbs, 1983: The mesoscale and microscale structure and organization of clouds and precipitation in midlatitude cyclones. VII: A model for the “seeder-feeder” process in warm-frontal rainbands. *J. Atmos. Sci.*, **40**, 1185–1206, [https://doi.org/10.1175/1520-0469\(1983\)040<1185:TMAMSA>2.0.CO;2](https://doi.org/10.1175/1520-0469(1983)040<1185:TMAMSA>2.0.CO;2).
- Schoenberg Ferrier, B., 1994: A double-moment multiple-phase four-class bulk ice scheme. Part I: Description. *J. Atmos. Sci.*, **51**, 249–280, [https://doi.org/10.1175/1520-0469\(1994\)051<0249:ADMPF>2.0.CO;2](https://doi.org/10.1175/1520-0469(1994)051<0249:ADMPF>2.0.CO;2).
- Skamarock, W. C., and Coauthors, 2008: A description of the Advanced Research WRF version 3. NCAR Tech. Note NCAR/TN-475+STR, 113 pp., <https://doi.org/10.5065/D68S4MVH>.
- Skofronick-Jackson, G., and Coauthors, 2017: The Global Precipitation Measurement (GPM) Mission for Science and Society. *Bull. Amer. Meteor. Soc.*, **98**, 1679–1695, <https://doi.org/10.1175/BAMS-D-15-00306.1>.
- Stoelinga, M. T., and Coauthors, 2003: Improvement of microphysical parameterization through observational verification experiment. *Bull. Amer. Meteor. Soc.*, **84**, 1807–1826, <https://doi.org/10.1175/BAMS-84-12-1807>.
- Tao, W.-K., J.-P. Chen, Z. Li, C. Wang, and C. Zhang, 2012: Impact of aerosols on convective clouds and precipitation. *Rev. Geophys.*, **50**, RG2001, <https://doi.org/10.1029/2011RG000369>.
- Thompson, G., and T. Eidhammer, 2014: A study of aerosol impacts on clouds and precipitation development in a large

- winter cyclone. *J. Atmos. Sci.*, **71**, 3636–3658, <https://doi.org/10.1175/JAS-D-13-0305.1>.
- , P. R. Field, R. M. Rasmussen, and W. D. Hall, 2008: Explicit forecasts of winter precipitation using an improved bulk microphysics scheme. Part II: Implementation of a new snow parameterization. *Mon. Wea. Rev.*, **136**, 5095–5115, <https://doi.org/10.1175/2008MWR2387.1>.
- Tokay, A., P. G. Bashor, and V. L. McDowell, 2010: Comparison of rain gauge measurements in the mid-Atlantic region. *J. Hydrometeor.*, **11**, 553–565, <https://doi.org/10.1175/2009JHM1137.1>.
- Wang, J., B. L. Fisher, and D. B. Wolff, 2008: Estimating rain rates from tipping-bucket rain gauge measurements. *J. Atmos. Oceanic Technol.*, **25**, 43–56, <https://doi.org/10.1175/2007JTECHA895.1>.
- Warner, M. D., C. F. Mass, and E. P. Salathé, 2012: Wintertime extreme precipitation events along the Pacific Northwest coast: Climatology and synoptic evolution. *Mon. Wea. Rev.*, **140**, 2021–2043, <https://doi.org/10.1175/MWR-D-11-00197.1>.
- Woods, C. P., M. T. Stoelinga, and J. D. Locatelli, 2007: The IMPROVE-1 storm of 1–2 February 2001. Part III: Sensitivity of a mesoscale model simulation to the representation of snow particle types and testing of a bulk microphysical scheme with snow habit prediction. *J. Atmos. Sci.*, **64**, 3927–3948, <https://doi.org/10.1175/2007JAS2239.1>.
- Zagrodnik, J. P., L. A. McMurdie, and R. A. Houze, 2018: Stratiform precipitation processes in cyclones passing over a coastal mountain range. *J. Atmos. Sci.*, **75**, 983–100, <https://doi.org/10.1175/JAS-D-17-0168.1>.
- Zhu, Y., and R. E. Newell, 1994: Atmospheric rivers and bombs. *Geophys. Res. Lett.*, **21**, 1999–2002, <https://doi.org/10.1029/94GL01710>.
- , and —, 1998: A proposed algorithm for moisture fluxes from atmospheric rivers. *Mon. Wea. Rev.*, **126**, 725–735, [https://doi.org/10.1175/1520-0493\(1998\)126<0725:APAFMF>2.0.CO;2](https://doi.org/10.1175/1520-0493(1998)126<0725:APAFMF>2.0.CO;2).